Journal of Pharmaceutical and Biomedical Analysis 114 (2015) 176–183

Journal of Pharmaceutical and Biomedical Analysis

journal homepage: www.elsevier.com/locate/jpba

Mapping the solid-state properties of crystalline lysozyme during pharmaceutical unit-operations

Mohammad Amin Mohammad [a,b,c,*], Ian M. Grimsey [c,1], Robert T. Forbes [c,2]

[a] Department of Pharmacy and Pharmacology, University of Bath, Bath BA2 7AY, UK
[b] Faculty of Pharmacy, University of Damascus, Damascus, Syria
[c] School of Pharmacy, University of Bradford, Bradford BD7 1DP, UK

ARTICLE INFO

Article history:
Received 4 April 2015
Received in revised form 11 May 2015
Accepted 13 May 2015
Available online 22 May 2015

Keywords:
Crystalline-amorphous-denatured transformations
Differential scanning calorimetry
FT-Raman
Lysozyme crystals
Milling
X-ray powder diffraction

ABSTRACT

Bulk crystallisation of protein therapeutic molecules towards their controlled drug delivery is of interest to the biopharmaceutical industry. The complexity of biotherapeutic molecules is likely to lead to complex material properties of crystals in the solid state and to complex transitions. This complexity is explored using batch crystallised lysozyme as a model. The effects of drying and milling on the solid-state transformations of lysozyme crystals were monitored using differential scanning calorimetry (DSC), X-ray powder diffraction (XRPD), FT-Raman, and enzymatic assay. XRPD was used to characterise crystallinity and these data supported those of crystalline lysozyme which gave a distinctive DSC thermogram. The apparent denaturation temperature (T_m) of the amorphous lysozyme was ~201 °C, while the T_m of the crystalline form was ~187 °C. Raman spectra supported a more α-helix rich structure of crystalline lysozyme. This structure is consistent with reduced cooperative unit sizes compared to the amorphous lysozyme and is consistent with a reduction in the T_m of the crystalline form. Evidence was obtained that milling also induced denaturation in the solid-state, with the denatured lysozyme showing no thermal transition. The denaturation of the crystalline lysozyme occurred mainly through its amorphous form. Interestingly, the mechanical denaturation of lysozyme did not affect its biological activity on dissolution. Lysozyme crystals on drying did not become amorphous, while milling-time played a crucial role in the crystalline-amorphous-denatured transformations of lysozyme crystals. DSC is shown to be a key tool to monitor quantitatively these transformations.

1. Introduction

Lysozymes are a group of enzymes defined as 1,4-β-*N*-acetylmuramidases cleaving the glycosidic bond in the bacterial peptidoglycan. Hen egg white lysozyme (HEWL) is a single chain polypeptide of 129 amino acids cross-linked with four disulfide bridges resulting in a molecular weight of 14307 Da [1]. HEWL has the ability to lyse bacteria, and therefore it has particular interest for application in food and pharmaceutical products [2]. Previous researchers assured its potent antimicrobial efficiency [3] and its safety [4]. Also, other research has resulted in improved intranasal absorption and delivery [5] and lung delivery [6].

Zhou et al. [7] made lysozyme containing mats and they verified its excellent antibacterial activity against *Escherichia coli* and *Staphylococcus aureus*, and therefore, these mats have promising uses in antimicrobial packing, tissue engineering, and wound dressing. Sax and Winter [8] prepared sustained release lysozyme containing implants using hot melt extrusion. Schlocker et al. [9] used milling to prepare protein-loaded microparticles in industrial quantities. Milling has also been used to prepare protein particles suitable for pulmonary delivery [10]. However, milling and other pharmaceutical processes (e.g., drying, mixing) may produce uncontrollable variation of protein solid states (i.e., crystal structure and crystal habit) and also loss of protein activity [11]. Different lyophilized solid forms of proteins have been shown to produce different dissolution rates for reconstitution [12]. The stability of crystalline lysozyme has been shown to be greater than that of the amorphous form [13,14]. Therefore, it is essential to monitor the solid state transformations of lysozyme during pharmaceutical processes.

Differential scanning calorimetry (DSC) is a well-established and widely used technique to monitor solid state transformations.

* Corresponding author at: Department of Pharmacy and Pharmacology, University of Bath, Bath BA2 7AY, UK. Tel.: +44 0 1225 386797.
E-mail addresses: mam71@bath.ac.uk, mamoham1@hotmail.co.uk (M.A. Mohammad), i.m.grimsey@bradford.ac.uk (I.M. Grimsey), r.t.forbes@bradford.ac.uk (R.T. Forbes).
[1] Tel: +44 0 1274 234754.
[2] Tel.: +44 0 1274 234653.

http://dx.doi.org/10.1016/j.jpba.2015.05.011
0731-7085/

However, the thermal transitions of lysozyme, in common with other proteins, are usually characterized in the solution state, and often using a high-sensitivity differential scanning calorimeter (HSDSC), which is capable of detecting the small changes in enthalpy that arise when proteins unfold within their solutions [15]. Modulated temperature differential scanning calorimetry [16] and thermally stimulated depolarized current [17] have been tested as alternatives. However, the thermal transitions in the solution state cannot differentiate the different solid forms. Therefore, researchers have studied the thermal transitions of lysozyme in solid state using conventional solid-state DSC. However, their results did not recognize the discrepancy between the thermal behaviours of the amorphous and crystalline lysozyme powders [13,14,18,19].

There is a renewed interest in lysozyme, and its solid state form can have a significant effect on dissolution and stability. We wished to explore how pre-treatment of lysozyme crystals affected thermal behaviour, in an attempt to use thermal profiles as a fingerprinting indicator of prior treatment. In this study, we prepare lysozyme crystals to be dried and/or milled, and appropriate mixtures of the treated forms were prepared. Our aim is to use DSC to monitor the potential solid state transformations of lysozyme during the treatment processes. We use Powder X-ray diffraction (PXRD), FT-Raman, and enzymatic assay for reference. To our knowledge this is the first application of DSC for the quantitative detection of crystalline, amorphous and denatured lysozyme forms.

2. Materials and methods

2.1. Materials

Hen egg-white lysozyme (HEWL) (purity; 95%) (Biozyme Laboratories, UK), *Micrococcus lysodeikticus* (Sigma-Aldrich), sodium chloride (NaCl) (99.5%) (Sigma-Aldrich) and sodium acetate anhydrous (purity; 98%) (BDH Chemicals Ltd., Poole, UK) were purchased as indicated. The purchased lysozyme sample was considered to be unprocessed lysozyme. Water was deionised and double distilled.

2.2. Sample preparation

2.2.1. Preparation lysozyme crystals using batch crystallization method

One litre of a solution of lysozyme 4% w/v in sodium acetate buffer (pH 4.6; 0.1 M) and one litre of a solution of sodium chloride 10% w/v in the same buffer were separately passed through a 0.2 micron filter and then mixed in a glass container. The produced solution contained 2% w/v lysozyme and 5% w/v NaCl. This solution was then sealed and kept for ten days at 20 °C. Crystals formed were collected by filtration. Adsorbed water was removed by air drying (5 h). These procedures were used to prepare lysozyme crystals by a batch crystallisation method [13].

2.2.2. Preparation of dried lysozyme crystals

A glass column of dimensions 2 m (three loops) × 6 mm (outer diameter) × 4 mm (inner diameter), was packed with lysozyme crystals. Anhydrous nitrogen gas was passed through the packed column at a flow rate of 10 ml/min, 30 °C and zero relative humidity for 10 days.

2.2.3. Preparation of milled dried lysozyme powders

Milling was achieved by rotating a marble pestle over the powder within a marble mortar at ~45 cycles per minute (cpm). Milling times of 3, 10, 20, 30, 45, and 60 min were used to produce different samples of milled dried crystals, named 3 M, 10 M, 20 M, 30 M, 45 M, and 60 M, respectively. Another two batches of 3 M, 10 M, 20 M and 60 M were also prepared for reference.

2.2.4. Preparation of amorphous lysozyme powders with different salt content

Precipitated samples were also prepared to explain the effect of NaCl on thermal behaviour of lysozyme particles. These amorphous samples were prepared using the same principle of batch crystallization method. Hence solutions containing 2% w/v lysozyme plus different amount of NaCl (0, 0.096, 0.16, and 0.8% w/v) in deionised water were dried under vacuum at a temperature 30 °C for two days to produce lysozyme powders theoretically containing 0, 24, 40 and 200 NaCl molecules for each lysozyme molecule, respectively. These four lysozyme samples were named P0, P24, P40, and P200, respectively, and their amorphous nature was confirmed by XRPD.

2.2.5. Preparation of lysozyme mixtures from two different samples

Unprocessed lysozyme and the 3 M sample were mixed at different ratios (w/w) of 3:7, 5:5, and 7:3 in 100 mg samples. The mixtures were lightly mixed in a mortar with a spatula for 10 min and then in a small plastic bag for 10 min to ensure their homogeneity.

2.3. Microscopy

A Zeiss Axioplan2 polarizing microscope (Carl Zeiss Vision GmbH; Hallbergmoos, Germany) was used to visualize the samples. The accompanying software (Axio Vision 4.2) was then used to determine the projected area diameters of the powders.

2.4. Thermogravimetric analysis (TGA)

The water content of each sample was estimated using Thermo Gravimetric Analysis (TGA 7 Perkin Elmer Ltd., Beaconsfield, UK). Samples of 3–10 mg were heated from 30 °C to 210 °C at a scan rate of 10 °C/min in aluminium pan under nitrogen flow at 20 ml/min. Each sample was analysed in triplicate. The decrease in the weight before decomposition was calculated and was considered as water content. TGA results were validated by re-analyzing the water content of some samples using Karl Fischer Titration (KFT) (701 KF Titrino with 703 Ti stand, Metrohm, Switzerland). Using TGA instead of KFT is that only a few mg is enough for TGA.

2.5. Powder X-ray diffraction (PXRD)

X-ray powder diffraction patterns of the powders were obtained using a Siemens D5000 diffractometer (Siemens, Karlsruhe, Germany), using Cu$K\alpha$ radiation (λ = 1.5418 Å). The generator was set to 40 kV and 30 mA. Samples were placed into plastic sample holder with zero background and levelled using a glass cover slide. Samples were scanned over an angular range of 2–10° (2θ), with a step size of 0.001° and a count time of 3 s per step. The sample stage was spun at 30 rpm. The instrument was calibrated prior to use, using a silicon standard.

2.6. Differential scanning calorimetry (DSC)

Differential scanning calorimetry (DSC) thermograms were obtained using a Perkin-Elmer Series 7 DSC (Perkin-Elmer Ltd., Beaconsfield, UK). Samples (4–7 mg) were sealed in aluminium pans. The escape of water was facilitated by placing a pinhole in the lid prior to sealing. The samples were equilibrated at 30 °C and heated to 210 °C at a scan rate of 10 °C/min under a flow of anhydrous nitrogen (20 ml/min). Each sample was analysed in triplicate. The

temperature axis and cell constant of the DSC cell were calibrated with indium (10 mg, 99.999% pure, melting point 156.60 °C, and heat of fusion 28.40 J/g).

2.6.1. Evaluation of microcalorimetric data

T_m and calorimetric transition enthalpies (ΔH_{Cal}) were measured by DSC, and then the cooperative unit size (n') was calculated after baseline correction using the following equation:

$$n' = \frac{\Delta H_{vH}}{\Delta H_{Cal}} \quad (1)$$

where ΔH_{vH} is the corresponding van't Hoff enthalpy of the unfolding. Bammel et al. [20] indicated that ΔH_{vH} can be obtained from:

$$\Delta H_{vH} = \frac{4RT_m^2 \Delta C_p(\max)}{\Delta H_{Cal}} \quad (2)$$

where R is the universal gas constant (8.314×10^{-3} kJ/K/mol), $\Delta C_p(\max)$ is the maximum heat capacity and it is calculated from:

$$\Delta C_p(\max) = \frac{\text{peak height}}{(\text{scan rate} \times \text{sample weight})} \quad (3)$$

2.7. FT-Raman spectroscopy

FT-Raman spectra of samples were recorded with a Bruker IFS66 optics system using a Bruker FRA 106 Raman module. The excitation source was an Nd:YAG laser operating at 1064 nm and a laser power of 50 mW was used. The FT-Raman module is equipped with a liquid nitrogen cooled germanium diode detector with an extended spectrum band width covering the wave number range 1800–450 cm^{-1}. Samples were placed in stainless steel sample cups and scanned 200 times with the resolution set at 8 cm^{-1}. The observed band wave numbers were calibrated against the internal laser frequency and are correct to better than ±1 cm^{-1}. The spectra were corrected for instrument response. The experiments were run at a controlled room temperature of 20±1 °C.

2.8. Enzymatic assay

Lysozyme catalyzes the hydrolysis of β-1,4-glycosidic linkages of cell-wall mucopolysaccharides [18]. This principle was used to measure the activity of lysozyme as follows. 30 μl of lysozyme solution 0.05% in phosphate buffer (pH = 5.2; 10 mM) was added to 2.97 ml substrate bacterial suspension 0.025% of *M. lysodeikticus* in phosphate buffer (pH = 6.24; 66 mM). The decrease in the absorption at 450 nm was monitored by using a UV–vis spectrophotometer (Pu 8700, Philips, UK). The activity was determined by measuring the decrease in the substrate bacterial suspension concentration with time. Hence the slope of the reduction in the light absorption at 450 nm against the time of 3 min, starting when the protein solutions were mixed with the substrate bacterial suspension, was considered to be the indicator of the activity [21]. The measurements were performed in controlled temperature room at 20 °C to avoid fluctuation of lysozyme activity. The concentrations of the protein solutions had been determined prior to the activity tests using the following equation.

$$[\text{Protein}] = \frac{\text{Abs}_{280\ \text{nm}}}{E_{280\ \text{nm}}} \quad (4)$$

where [protein] is the concentration of protein in the tested solution w/v%, $\text{Abs}_{280\ \text{nm}}$ is the absorption of the tested protein solution at 280 nm, $E_{280\ \text{nm}}$ is the absorption of protein standard solution with concentration 0.05 w/v%. The concentrations of the solutions were diluted to be about 0.05% w/v so as to give absorption of less than 0.8. The activities of all samples were measured relative to that of a corresponding fresh sample, which was considered as the standard solution.

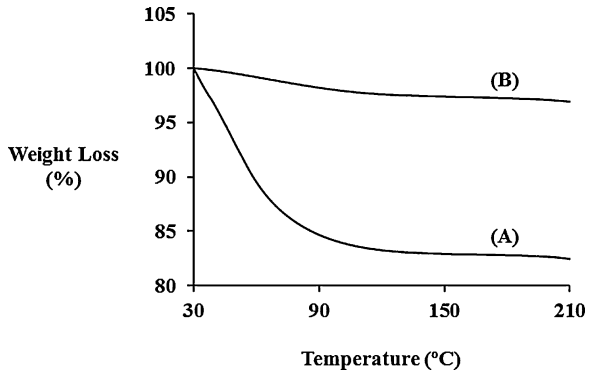

Fig. 1. Example TGA thermograms of lysozyme (A) crystals (B) dried crystals. Conditions: samples heated from 30 to 210 °C; heating rate: 10 °C/min.

3. Results and discussion

3.1. Microscopy

Fig. S1 shows the photomicrograph of a lysozyme crystal. The anisotropic crystals exhibited a birefringence phenomenon when viewed under a polarizing microscope. The elongated prism-like crystals were in general of a projected area diameter of ~1200 μm (Fig. S1). Their shape was consistent with their preparation temperature, which was 20 °C. The crystal shape of lysozyme is known to be affected by temperature, and a temperature of ~20 °C usually results in elongated prism-like crystals [22]. Samples 3 M, 10 M, 20 M, and 30 M had diameters of ~80 μm (Fig. S2), ~7 μm (Fig. S3), ~2.5 μm (Fig. S4), and less than 1 μm (Fig. S5), respectively.

3.2. Thermogravimetric analysis (TGA)

The results of TGA analysis were used to estimate the water content of the crystal forms. The thermograms (Fig. 1) indicate that on drying using the conditions described above, the water content decreased from 17.3 ± 1.0% w/w to 2.6 ± 0.3% w/w. The obtained values of water content in protein powders using TGA were previously shown to be consistent with Karl Fischer titration data [13].

3.3. X-ray powder diffraction (XRPD)

The diffractogram presented in Fig. 2A shows an absence of diffraction peaks for the unprocessed lysozyme powder indicating that it was amorphous. However, in Fig. 2B diffraction peaks for the lysozyme crystals at 2θ angles less than 8° are present. Proteins are large molecules and are crystallized typically in unit cells having high d values, and so according to Bragg's law, lysozyme crystals are expected to diffract X-ray at low 2θ angles.

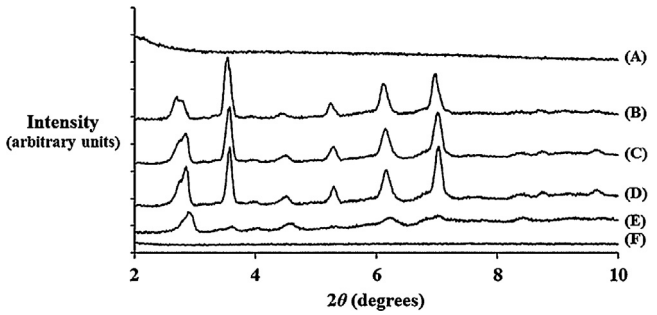

Fig. 2. PXRD patterns of lysozyme powders (A) unprocessed, (B) crystals, (C) dried crystals, (D) dried crystals milled for 3 min (3 M), (E) dried crystals milled for 10 min (10 M), and (F) dried crystals milled for 20 min (20 M).

Because lysozyme crystals exist in different forms, the CMPR program (Version 1.32) [23] was employed for phase identification. The observed PXRD peaks of the crystals at 2.82°, 3.56°, 4.47°, 5.21°, 6.09°, and 6.97° (Fig. 2B) fitted the faces (*H*,*K*,*L*) {(1,1,1), (3,1,0), (4,0,0), (4,1,1), (4,3,1), (5,3,1)} of the tetragonal form of lysozyme with parameters $A = 78.54$, $B = 78.54$ and $C = 37.77$, $\alpha = \beta = \gamma = 90°$ taken from protein data bank reference number 193L [24].

Dried lysozyme crystals were also characterised using PXRD and data indicated that the degree of crystallinity was predominantly maintained. The fact that the intensity of the XRPD peaks, which did not notably change (Fig. 2C), was evidence to this effect. Minor up shifting in the diffracted peaks after drying was noticed. This can be due to shrinkage of the unit cell to lower d values upon dehydration. The cell volume of tetragonal lysozyme crystals shrunk under the effect of pressure without a loss in its diffraction property [25]. Our XRPD finding agrees with previous results. For example, both monoclinic and triclinic crystals of HEWL have been shown to maintain their ability to diffract X-rays after dehydration [26,27], respectively. However, it contradicts some previous low frequency Raman spectra results, which showed that tetragonal lysozyme crystals resulted in crystallinity loss and conversion into an isotropic material (amorphous) after drying from ~33.5% w/w to ~9% w/w water content by equilibrating at ~30% r.h. [28,29]. In general, although dehydration firstly transfers a protein crystal to a metastable state, which then collapses and loses its packing structure, some crystals survive their crystallinity upon dehydration [26]. The findings of the present study would suggest that the conditions of the drying process would play an important part as to whether crystallinity is maintained. Thus if protein crystals are to be used as a drug delivery vehicle after bulk crystallisation then the subsequent milling and drying conditions will require close control and monitoring to obtain consistent results.

Milling of the dried crystals did produce a loss in crystallinity. XRPD was able to follow the loss of crystallinity of dried lysozyme crystals with comminution time. In case of 3 M, the 3 min of milling did not induce crystallinity loss (Fig. 2D) as indicated by PXRD. However, the intensity of the diffracted peaks of sample 10 M decreased (Fig. 2E). This indicates that lysozyme crystals became partially disordered after only 10 min of milling. Fig. 2F shows that 20 min of milling was sufficient to produce a diffractogram with no clear peaks for the 20 M sample, and so its XRPD spectrum became similar to that of the amorphous lysozyme (unprocessed) (Fig. 2A) which is consistent with transformation to the amorphous state.

3.4. Differential scanning calorimetry (DSC)

Lysozyme DSC thermograms, in the solid state, typically show two endothermic peaks. The broad peak ranging from ~30 to ~140 °C is due to water removal, and its area depends on the water residue in the samples. The second peak at ~200 °C, and its peak maximum was considered to reflect the apparent denaturation temperature (T_m) [13,14,18,19,30]. Fig. 3A shows a typical lysozyme thermogram demonstrating the presence of peaks at similar positions to those mentioned above. Thermograms for all other samples show a consistent water removal peak. However, the position and magnitude of T_m peak was found to depend on the solid state form of the lysozyme powder. The differences observed from DSC analysis align with the differences between the states previously observed by XRPD (Fig. 2). Amorphous lysozyme obtained as received (unprocessed lysozyme) thermally peaked at a T_m of about ~201 °C (Fig. 3A), while samples of crystalline lysozyme (crystals, dried crystals, or the minimally milled 3 M sample) gave a lower T_m of about ~187 °C (Fig. 4B–D). Evidence that the 10 M sample was transformed partially to an amorphous form was apparent from inspection of the DSC thermal scan since it contained two distinct T_m's consistent with amorphous and crystalline lysozyme forms

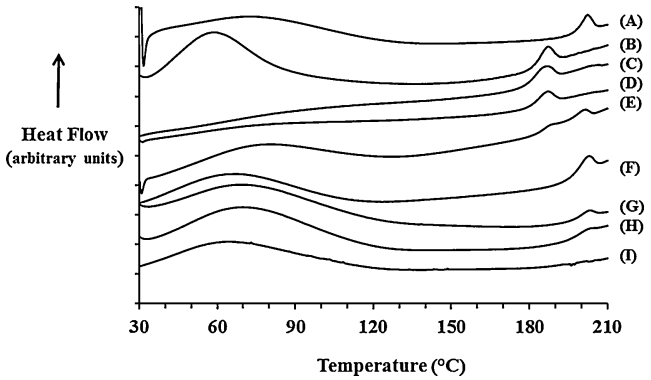

Fig. 3. Example DSC thermograms of lysozyme (A) unprocessed, (B) crystals, (C) dried crystals, (D) dried crystals milled for 3 min (3 M), (E) dried crystals milled for 10 min (10 M), (F) dried crystals milled for 20 min (20 M), (G) dried crystals milled for 30 min, (H) dried crystals milled for 45 min (45 M), and (I) dried crystals milled for 60 min (60 M). Conditions: samples heated from 30 to 210 °C; heating rate: 10 °C/min.

respectively at separate T_m of ~187 and ~201 °C (Fig. 3E). Similar to the XPRD evidence above, DSC data suggested that further milling completed the amorphous transformation, with the 20 M sample being amorphous, and hence it only had the T_m of an amorphous state at ~201 °C (Fig. 3F).

Close scrutiny of the thermograms showed that for sample 20 M (amorphous lysozyme), T_m was slightly decreased by only ~1 °C compared to that of the other amorphous lysozyme (unprocessed sample). However, this small difference was significant (*t*-test: $P < 0.05$) (Table 1). This minor reduction is likely to be due to the presence of NaCl content in the former sample. The amount of NaCl in the lysozyme crystal is approximated to be ~10 NaCl molecules for each lysozyme molecule. At the preparation pH, each molecule of lysozyme needed ~10 Cl^- ions of NaCl to shield its positive charges, which induce the repulsion between lysozyme molecules. This shielding by counter ions of the precipitant (NaCl) is necessary to start nucleation and form crystals in which these ions are trapped [31]. The precipitated samples which were precipitated with different salt contents (P0, P24, P40, and P200) revealed a strong inverse relationship between salt content and T_m (correlation coefficient $r = -0.92$). The values of T_m were 202.2 ± 0.3, 200.3 ± 0.5, 198.2 ± 0.5, and 195.8 ± 0.2, respectively, and their DSC profiles and amorphous PXRD patterns are provided in supplementary data (Fig. S6 and Fig. S7). Therefore, according to this correlation, the presence of around 10 NaCl molecules for each lysozyme molecule reduces T_m by ~1 °C.

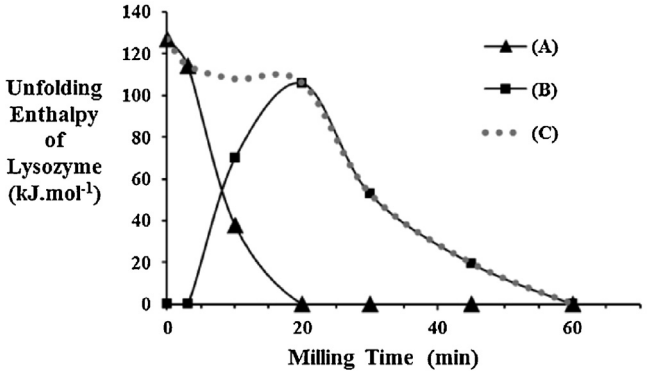

Fig. 4. Correlation between the milling time and the calorimetric unfolding enthalpies of the milled lysozyme crystals (A) the enthalpy of the crystalline content, (B) the enthalpy of the amorphous content and (C) the enthalpy of the total contents (crystalline and amorphous).

Table 1
Apparent denaturation temperature (T_m), calorimetric enthalpy (ΔH_{Cal}), Van't Hoff enthalpy (ΔH_{vH}), and cooperative unit (n') of lysozyme samples in the solid state; determined by differential scanning calorimetry (DSC). Conditions: samples heated from 30 to 210 °C; heating rate: 10 °C/min.

Lysozyme samples	T_m (°C)	ΔH_{Cal} (kJ/mol)	ΔH_{vH} (kJ/mol)	n'
Unprocessed	202.3 (0.5)	134.1 (4.6)	1400.9 (35.6)	10.4 (0.6)
Crystals	187.3 (0.3)	125.3 (7.2)	1045.9 (82. 6)	8.3 (0.7)
Dried crystals	187.8 (0.7)	127.0 (4.2)	1016.1 (39.7)	8.0 (0.5)
Milled dried crystal for 3 min (3 M)	187.9 (0. 6)	114.4 (1.2)	940.2 (79.1)	8.2 (0.8)
Milled dried crystal for 10 min (10 M)	187.5 (0.4)	38.0 (11.3)	307.9 (71.2)	8.1 (0. 5)
	201.1 (0.2)	69.9 (8.5)	762.6 (61.3)	10.9 (0.4)
Milled dried crystals for 20 min (20 M)	201.0 (0.4)	105.9 (3.6)	1180.1 (60.7)	11.1 (0.6)
Milled dried crystals for 30 min (30 M)	200.8 (0.6)	52.8 (7.5)	–	–
Milled dried crystals for 45 min (45 M)	201.1 (0.5)	19.6 (2.9)	–	–
Milled dried crystals for 60 min (60 M)	No peak	–	–	–

Values within parenthesis are standard deviation, $n = 3$.

The T_m of a protein does not necessarily represent a solid–liquid transformation. Proteins do not melt, but they change their molecular conformation from a native to denatured state at the T_m which overcomes the attractive intra-molecular forces, which preserve their native state. In solution state where lysozyme molecules are well separated from each other by water molecules, the T_m of lysozyme is ~76 °C [32]. The cooperative unit (n') is typically thought to estimate the lowest number of molecules which form an independently melting cluster of molecules within a sample [33] and is used as an indicator of the degree of unfolding cooperativity of lysozyme [15]. In solution state, n' of lysozyme solutions ranges from 1 to 2 (i.e., ~1.5) [34] Compared with the solution state, n' of lysozyme in the dried amorphous form (e.g. unprocessed or 20 M sample) was estimated to increase from ~1.5 to ~10.5, and this is associated with the increase in T_m from ~76 to ~201 °C (Table 1).

We can postulate that when the cooperative unit increases, a higher temperature is needed to unfold the lysozyme molecular aggregates, and that the larger the cooperative unit, the higher the T_m. The n' of the crystalline form (e.g. crystals, dried crystals, 3 M) was lower than those of the amorphous form by ~2.5 unit (t-test: $P < 0.05$) (Table 1). This explains the reduction in T_m of the crystalline form by ~14 °C compared to the amorphous form. Although the unfolding of proteins is an intra-molecular phenomenon rather than an inter-molecular phenomenon, the unfolding of a molecule within a molecular aggregate is resisted by the steric hindrance and repulsion of the other molecules in the unit.

Table 1 and Fig. 3 show that milling decreased the ΔH_{Cal} of the unfolding peak of the crystalline form (ΔH_{Cal}^{Cr}) with a corresponding increase in the ΔH_{Cal} of the unfolding peak of the amorphous form (ΔH_{Cal}^{Am}). When ΔH_{Cal}^{Cr} vanished, ΔH_{Cal}^{Am} reached a maximum of 105.9 kJ/mol (as in the case of 20 M sample), which is lower than those of both the crystalline form (dried crystals) and the amorphous form (unprocessed sample). Therefore, the complete crystalline-amorphous transformation associated with slightly mechanical denaturation (~17%). The further milling denatured gradually the amorphous form, as ΔH_{Cal}^{Am} decreased gradually by milling (i.e., 30 M and 45 M samples). Prolonged milling of dried crystals produced thermal evidence of a loss of unfolding due to the absence of a T_m as in the case of 60 M (Fig. 3I). Fig. 4 summarizes the correlation between the milling time and the calorimetric unfolding enthalpies of the crystalline and amorphous peaks. This observation coupled with the milling data discussed above is suggestive that milling initially induced a partial crystalline-amorphous transformation, followed by a complete amorphization transformation, and then on subsequent prolonged milling produced complete mechanical denaturation. Although a small part of lysozyme molecules denatured during the crystalline-amorphous transformation, the mechanical denaturation of crystalline lysozyme mainly goes through amorphous state. Similarly, the other two batches of 3 M, 10 M, 20 M and 60 M verified the crystalline-amorphous-denatured transformations of lysozyme powders during milling and the distinctive thermal behaviours of each form (Table 2).

3.4.1. Quantitative analysis of lysozyme solid states by DSC

Conventional DSC has been used to estimate the different solid phases in lactose powders. The estimation depended on knowing the enthalpy of solid phase transformation for each form. This DSC approach has been previously verified [35].

Applying the same approach to monitor the processing of the lysozyme powders, crystalline lysozyme (i.e. crystals) and amorphous lysozyme (i.e. unprocessed powder) produced similar enthalpies (t-test: $P > 0.05$), with an average of 125 and 134 kJ/mol, respectively. Therefore, these values were considered as the enthalpy of the native solid lysozyme. We assume that milled solid lysozyme powders would consist of mixtures of crystalline, amorphous and/or denatured lysozyme. The percentages of crystalline form (Cr%), amorphous form (Am%), and denatured form (De%) in the lysozyme powders can be determined from:

$$\mathrm{Cr\%} = \left(\frac{\Delta H_{Cal}^{\sim 187}}{125}\right) \times 100 \quad (5)$$

$$\mathrm{Am\%} = \left(\frac{\Delta H_{Cal}^{\sim 201}}{134}\right) \times 100 \quad (6)$$

$$\mathrm{De\%} = 100 - (\mathrm{Cr\%} + \mathrm{Am\%}) \quad (7)$$

Table 2
Apparent denaturation temperature (T_m), calorimetric enthalpy (ΔH_{Cal}) of the second and third batches of the milled lysozyme samples (3 M, 10 M, 20 M and 60 M); determined by differential scanning calorimetry (DSC). Conditions: samples heated from 30 to 210 °C; heating rate: 10 °C/min.

Lysozyme samples	Second batch		Third batch	
	T_m (°C)	ΔH_{Cal} (kJ/mol)	T_m (°C)	ΔH_{Cal} (kJ/mol)
Milled dried crystal for 3 min (3 M)	187.4 (1.1)	122.3 (3.7)	188.4 (0.7)	119.7 (8.9)
Milled dried crystal for 10 min (10 M)	188.2 (0.7)	48.9 (6.2)	187.1 (0.9)	37.4 (3.6)
	200.9 (0.5)	64.8 (5.9)	200.1 (1.2)	74.9 (7.1)
Milled dried crystals for 20 min (20 M)	200.6 (0.9)	112.8 (4.6)	200.9 (0.8)	109.2 (5.2)
Milled dried crystals for 60 min (60 M)	No peak	–	No peak	–

Values within parenthesis are standard deviation, $n = 3$.

Table 3
Apparent denaturation temperature (T_m), calorimetric enthalpy (ΔH_{Cal}), and the percentages of crystalline (Cr%), amorphous (Am%), and denatured (De%) in the mixtures of amorphous lysozyme (unprocessed) and crystalline lysozyme (3 M) samples at different ratios; determined by differential scanning calorimetry (DSC). Conditions: samples heated from 30 to 210 °C; heating rate: 10 °C/min.

Mixtures	Crystalline Peak		Amorphous peak		Cr%	Am%	De%
	T_m (°C)	ΔH_{Cal} (kJ/mol)	T_m (°C)	ΔH_{Cal} kJ/mol			
Unprocessed/3 M (3:7)	187.1 (0.7)	79.1 (8.0)	201.8 (0.4)	41.8 (6.0)	63.3 (6.4)	31.2 (4.5)	5.5 (1.6)
Unprocessed/3 M (5:5)	188.1 (0.5)	58.6 (4.9)	202.1 (0.3)	63.4 (7.0)	46.9 (3.9)	47.3 (5.2)	5.8 (2.0)
Unprocessed/3 M (7:3)	187.6 (0.3)	43.5 (6.9)	202.2 (0.8)	82.5 (8.7)	34.8 (5.5)	61.6 (6.5)	3.6 (1.4)

Values within parenthesis are standard deviation, $n = 3$.

where $\Delta H_{Cal}^{\sim 187}$ and $\Delta H_{Cal}^{\sim 201}$ are the measured enthalpy (kJ/mol) of the unfolding peaks at T_m of ~187 and ~201 °C, respectively.

To test the quantitative hypothesis amorphous lysozyme (unprocessed sample) and crystalline lysozyme (3 M sample) were mixed at different ratios of 3:7, 5:5, and 7:3 and then they analysed by DSC (same procedures). According to Eqs. (5)–(7), the amorphous sample contains 100% native lysozyme, but the crystalline sample, which had $\Delta H_{Cal}^{\sim 187} = 114.4$ kJ/mol, contains 91.5% native and 8.5% denature lysozyme. Therefore, the three mixtures of unprocessed: 3 M (3:7, 5:5 and 7:3) should contain (27.4%, 70.0%, 2.6%), (45.7%, 50.0%, 4.3%) and (64.0%, 30.0%, 6.0%) of (Cr%, Am%, and De%), respectively. These calculated crystalline, amorphous and denatured percentages using the above equations were similar to the actual percentages in the mixtures listed in Table 3. Fig. 5 shows the distinctive unfolding peaks of the crystalline and amorphous forms of the mixtures.

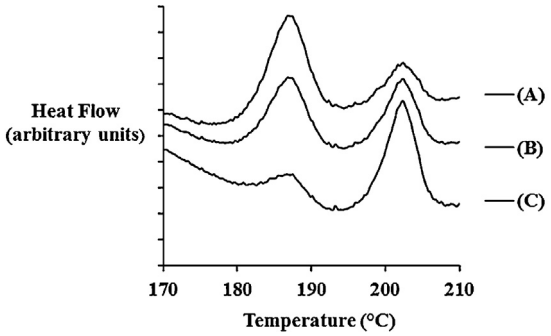

Fig. 5. Expanded DSC thermograms showing the unfolding transition peaks of mixtures of amorphous lysozyme (unprocessed): crystalline lysozyme (3 M) samples at different ratios of (A) 3:7, (B) 5:5, and (C) 7:3. Conditions: samples heated from 30 to 210 °C; heating rate: 10 °C/min.

3.5. FT-Raman study

Raman spectroscopy was used to compare the molecular conformation of crystalline (3 M sample), amorphous lysozyme (20 M sample) and extensively milled (denatured) lysozyme (60 M sample) with dried lysozyme crystals. The band at 1447 cm^{-1} indicates the CH bending vibrations of aliphatic side chains, and its intensity and position are unaffected by changes induced in protein structure after dehydration or applying different stresses [36]. Therefore, it was used as internal intensity standard to normalize Raman spectra before comparison (Fig. 6A).

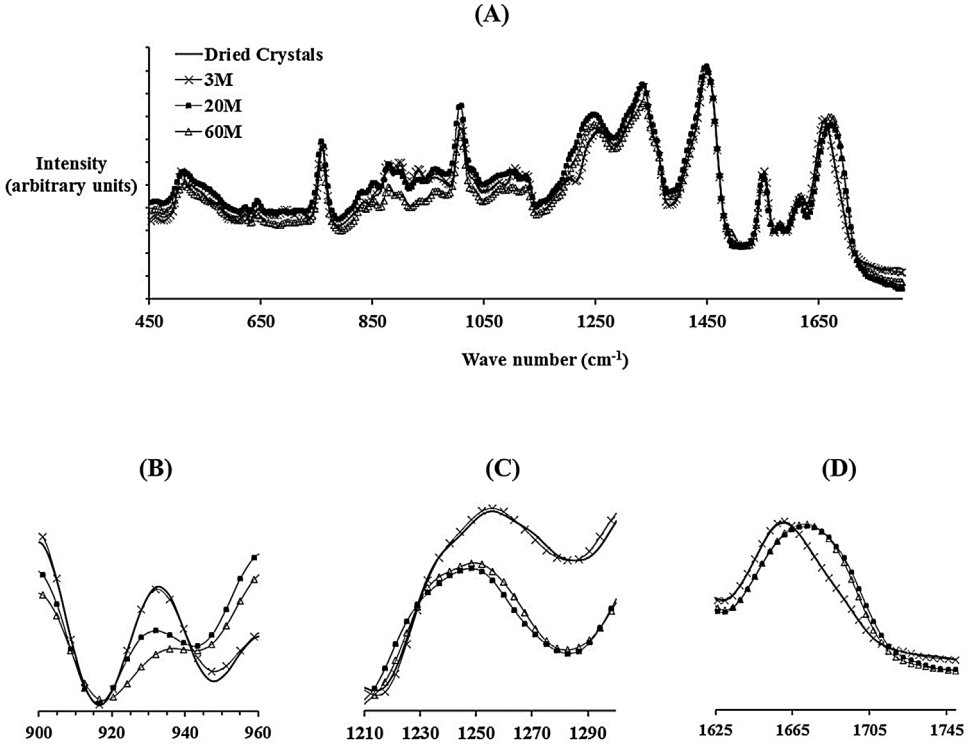

Fig. 6. FT-Raman spectra of dried crystals (line without marker), 3 M sample (crystalline lysozyme) (cross), 20 M sample (amorphous) (square) and 60 M (denatured lysozyme) (triangle). Vibration modes are (B) back bone, (C) amide III and (D) amide I. The spectra were normalized using the methylene deformation mode at 1448 cm^{-1} as an internal intensity standard.

Table 4
The effect of pharmaceutical operations including milling time on the enzymatic activity of lysozyme powders.

Lysozyme samples	% Activity
Unprocessed	100.0 (1.5)
Crystals	102.3 (2.0)
Dried crystals	100.1 (2.9)
Milled dried crystal for 3 min (3 M)	100.4 (1.8)
Milled dried crystal for 20 min (20 M)	101.3 (2.7)
Milled dried crystals for 60 min (60 M)	99.9 (1.6)

Values within parenthesis are standard deviation, $n = 3$.

Compared to the amorphous form of lysozyme (20 M sample), the crystalline form (dried crystals and 3 M sample) showed greater intensity of the νCa—C—N mode at 930 cm^{-1} (Fig. 6B), and produced a higher vibration mode of amide III (N—H in-plane bend + C—N stretch) at ~1265 cm^{-1} (Fig. 6C) and a lower and sharper vibration mode of amide I (C=O stretch) at ~1660 cm^{-1} (Fig. 6D). The intensity of νCa—C—N mode at 930 cm^{-1} [37], upshifting of amide III (N—H in-plane bend +C—N stretch) [38], and downshifting and sharpening of the line of amide I (C=O stretch) at ~1660 cm^{-1} [39] indicates a higher α-helix content. This means that the crystalline form maintained the α-helix structure of native lysozyme more than the amorphous form. The native secondary structure of lysozyme consists of three alpha helix regions extending 5–15, 24–34 and 88–96 amino acid residues [24].

Rich α-helix structures have a low tendency to aggregate compared to rich β-sheet structures [15]. This possibly explains why the crystalline form had less tendency to thermally unfold in lower n' compared to the amorphous form. Therefore, according to our above postulation, the spectroscopic observation that the crystalline form contains more alpha helix may explain why the crystalline lysozyme unfolded at lower T_m.

Comparison of the spectrum of the denatured lysozyme (sample 60 M) with that of the amorphous form shows that mechanical denaturation induced further reduction in the intensity of νCa—C—N mode at 930 cm^{-1} (Fig. 6B), which in turn implies a further reduction in α-helix content.

3.6. Enzymatic assay

Interestingly, milled samples did not show a reduction in biological activity (ANOVA: $P > 0.05$) (Table 4). The ability of lysozyme to re-nature on dissolution is a possible explanation for this finding. Indeed, previous research has shown the strong refolding ability of lysozyme upon dissolution in aqueous media [40]. Likewise, despite significant loss of the Raman vibrations of lysozyme upon denaturation by γ-irradiation, the denatured lysozyme samples almost fully recovered their biological activity on dissolution [39].

4. Conclusions

Bulk crystallisation of protein therapeutic molecules for controlled drug delivery studies is of interest to the biopharmaceutical industry. The complexity of biotherapeutic molecules is likely to lead to complex material properties of crystals in the solid state. Here we exemplify, using the model drug lysozyme, the effects of processing lysozyme crystals and are able to show distinct differences in the properties of the materials after processing which could be used in optimising and controlling processes for the purposes of quality by design.

By drying lysozyme crystals using a controlled method we were able to evidence the removal of water and maintain crystallinity. However, the size reduction of dried lysozyme crystals by milling was shown to promote formation of an amorphous solid-state form. Raman spectroscopy provided evidence that the amorphous form was then denatured in the solid state by further milling. The milling time was the critical attribute determining the extent of the transformations. DSC was successfully employed in monitoring the three different states of lysozyme (namely crystalline, amorphous, and denatured) in the solid state. The DSC thermogram of the crystalline lysozyme exhibited T_m at ~187 °C which was lower than that of amorphous lysozyme by ~14 °C. The mechanically denatured lysozyme did not provide a thermal unfolding transition. The calorimetric enthalpies of the crystalline and amorphous peaks were used to analyze quantitatively the three different states of lysozyme. XRPD data were consistent with the crystallinity of lysozyme identified by DSC. Interpretation of the Raman data from the same samples is consistent with a crystalline form having a lower tendency to aggregate due to its greater α-helix rich structure compared to the amorphous form. Significantly, although the molecular arrangement and molecular conformation of lysozyme changed during milling, its biological activity did not decrease. Clearly, subtle changes in solid-state processing conditions of crystalline lysozyme can bring about major changes in its solid-state properties. The effects of a wider range of milling variables, including different mill types, on lysozyme solid-state transformations and behaviour will be the subject of a future study.

Acknowledgements

The authors thank Dr Ian S. Blagbrough (University of Bath) for helpful discussions and Dr Colin Seaton (University of Bradford) for help in using the CMPR program. MAM gratefully acknowledges CARA (Zeid Al-Bayaty and Kate Robertson) for providing an academic fellowship.

Appendix A. Supplementary data

Supplementary data associated with this article can be found, in the online version, at doi:10.1016/j.jpba.2015.05.011

References

[1] W. Zhao, R. Yang, R. Lu, Y. Tang, W. Zhang, Investigation of the mechanisms of pulsed electric fields on inactivation of enzyme: lysozyme, J. Agric. Food Chem. 55 (2007) 9850–9858.
[2] E.A. Charter, G. Lagarde, Natural anti-microbial systems: lysozyme and other proteins in eggs, in: C.A. Batt (Ed.), Encyclopedia of Food Microbiology, Second ed., Elsevier, Ltd, San Diego, CA, 2014, pp. 936–940.
[3] M.I. Hoq, H.R. Ibrahim, Potent antimicrobial action of triclosan–lysozyme complex against skin pathogens mediated through drug-targeted delivery mechanism, Eur. J. Pharm. Sci. 42 (2011) 130–137.
[4] D. Cerven, G. DeGeorge, D. Bethell, 28-Day repeated dose oral toxicity of recombinant human apo-lactoferrin or recombinant human lysozyme in rats, Regul. Toxicol. Pharm. 51 (2008) 162–167.
[5] H.J. Cho, P. Balakrishnan, S.J. Chung, C.K. Shim, D.D. Kim, Evaluation of protein stability and in vitro permeation of lyophilized polysaccharides-based microparticles for intranasal protein delivery, Int. J. Pharm. 416 (2011) 77–84.
[6] O.N. Ógáin, J. Li, L. Tajber, O.I. Corrigan, A.M. Healy, Particle engineering of materials for oral inhalation by dry powder inhalers. I—Particles of sugar excipients (trehalose and raffinose) for protein delivery, Int. J. Pharm. 405 (2011) 23–35.
[7] B. Zhou, Y. Li, H. Deng, Y. Hu, B. Li, Antibacterial multilayer films fabricated by layer-by-layer immobilizing lysozyme and gold nanoparticles on nanofibers, Colloids Surf, B: Biointerfaces 116 (2014) 432–438.
[8] G. Sax, G. Winter, Mechanistic studies on the release of lysozyme from twin-screw extruded lipid implants, J. Controlled Release 163 (2012) 187–194.
[9] W. Schlocker, S. Gschließer, A. Bernkop-Schnürch, Evaluation of the potential of air jet milling of solid protein–poly (acrylate) complexes for microparticle preparation, Eur. J. Pharm. Biopharm. 62 (2006) 260–266.
[10] H. Hoyer, W. Schlocker, K. Krum, A. Bernkop-Schnürch, Preparation and evaluation of microparticles from thiolated polymers via air jet milling, Eur. J. Pharm. Biopharm. 69 (2008) 476–485.
[11] J.H. Kwon, C.W. Kim, A novel insulin microcrystals preparation using a seed zone method, J. Cryst. Growth 263 (2004) 536–543.
[12] C. Müller, J. Ulrich, The dissolution phenomenon of lysozyme crystals, Cryst. Res. Technol. 47 (2012) 169–174.
[13] A.A. Elkordy, R.T. Forbes, B.W. Barry, Integrity of crystalline lysozyme exceeds that of a spray-dried form, Int. J. Pharm. 247 (2002) 79–90.

[14] A.A. Elkordy, R.T. Forbes, B.W. Barry, Stability of crystallised and spray-dried lysozyme, Int. J. Pharm. 278 (2004) 209–219.
[15] H. Liu, P. Yin, S. He, Z. Sun, Y. Tao, Y. Huang, H. Zhuang, G. Zhang, S. Wei, ATP-induced noncooperative thermal unfolding of hen lysozyme, Biochem. Biophys. Res. Commun. 397 (2010) 598–602.
[16] A. Badkar, P. Yohannes, A. Banga, Application of TZERO calibrated modulated temperature differential scanning calorimetry to characterize model protein formulations, Int. J. Pharm. 309 (2006) 146–156.
[17] Y. Hirakura, H. Yamaguchi, M. Mizuno, H. Miyanishi, S. Ueda, S. Kitamura, Detection of lot-to-lot variations in the amorphous microstructure of lyophilized protein formulations, Int. J. Pharm. 340 (2007) 34–41.
[18] R.R. Haj-Ahmad, A.A. Elkordy, C.S. Chaw, A. Moore, Compare and contrast the effects of surfactants (Pluronic®F-127 and Cremophor®EL) and sugars (β-cyclodextrin and insulin) on properties of spray dried and crystallised lysozyme, Eur. J. Pharm. Sci. 49 (2013) 519–534.
[19] Z. Du, Y.X. Guan, S.J. Yao, Z.Q. Zhu, Supercritical fluid assisted atomization introduced by an enhanced mixer for micronization of lysozyme: particle morphology, size and protein stability, Int. J. Pharm. 421 (2011) 258–268.
[20] B.P. Bammel, D.D. Hamilton, R.P. Haugland, H.P. Hopkins, J. Schuette, W. Szalecki, J.C. Smith, NMR, calorimetric, spin-label, and optical studies on a trifluoromethyl-substituted styryl molecular probe in dimyristoylphosphatidylcholine vesicles and multilamellar suspensions: a model for location of optical probes, BBA-Biomembr. 1024 (1990) 61–81.
[21] D. Shugar, Measurement of lysozyme activity and the ultraviolet inactivation of lysozyme, Biochim. Biophys. Acta 8 (1952) 302.
[22] J. Lu, X.J. Wang, C.B. Ching, Batch crystallization of soluble proteins: effect of precipitant, temperature and additive, Prog. Cryst. Growth Charact. 45 (2002) 201–217.
[23] B.H. Toby, CMPR—a powder diffraction toolkit, J. Appl. Crystallogr. 38 (2005) 1040–1041.
[24] M.C. Vaney, S. Maignan, M. RiesKautt, A. Ducruix, High resolution structure (1.33 angstrom) of a HEW lysozyme tetragonal crystal grown in the APCF apparatus: data and structural comparison with a crystal grown under microgravity from SpaceHab-01 mission, Acta Crystallogr. D Biol. Crystallogr. 52 (1996) 505–517.
[25] C. Charron, M.C. Robert, B. Capelle, A. Kadri, G. Jenner, R. Giegé, B. Lorber, X-ray diffraction properties of protein crystals prepared in agarose gel under hydrostatic pressure, J. Cryst. Growth 245 (2002) 321–333.
[26] K. Harata, T. Akiba, Structural phase transition of monoclinic crystals of hen egg-white lysozyme, Acta Crystallogr. D: Biol. Crystallogr. 62 (2006) 375–382.
[27] G.S. Kachalova, V.N. Morozov, T.Y. Morozova, E.T. Myachin, A.A. Vagin, B.V. Strokopytov, Y.V. Nekrasov, Comparison of structures of dry and wet hen egg-white lysozyme molecule at 1.8 Å resolution, FEBS Lett. 284 (1991) 91–94.
[28] H. Urabe, Y. Sugawara, M. Ataka, A. Rupprecht, Low-frequency Raman spectra of lysozyme crystals and oriented DNA films: dynamics of crystal water, Biophys. J. 74 (1998) 1533–1540.
[29] A.B. Kudryavtsev, G. Christopher, C.D. Smith, S.B. Mirov, W.M. Rosenblum, L.J. DeLucas, The effect of ordering of internal water in thaumatin and lysozyme crystals as revealed by Raman method, J. Cryst. Growth 219 (2000) 102–114.
[30] W.L. Hulse, R.T. Forbes, M.C. Bonner, M. Getrost, Do co-spray dried excipients offer better lysozyme stabilisation than single excipients? Eur. J. Pharm. Sci. 33 (2008) 294–305.
[31] F. Rosenberger, Protein crystallization, J. Cryst. Growth 166 (1996) 40–54.
[32] A.A. Elkordy, R.T. Forbes, B.W. Barry, Study of protein conformational stability and integrity using calorimetry and FT-Raman spectroscopy correlated with enzymatic activity, Eur. J. Pharm. Sci. 33 (2008) 177–190.
[33] H. Lu, J.C. Wojtowicz, I.A. Butovich, Differential scanning calorimetric evaluation of human meibomian gland secretions and model lipid mixtures: transition temperatures and cooperativity of melting, Chem. Phys. Lipids 170 (2013) 55–64.
[34] N. Hassan, P.V. Verdes, J.M. Ruso, Assessment of interactions between four proteins and benzothiazole derivatives by DSC and CD, J. Chem. Thermodyn. 43 (2011) 399–404.
[35] W. Kaialy, G.P. Martin, M.D. Ticehurst, P. Royall, M.A. Mohammad, J. Murphy, A. Nokhodchi, Characterisation and deposition studies of recrystallised lactose from binary mixtures of ethanol/butanol for improved drug delivery from dry powder inhalers, AAPS J. 13 (2011) 30–43.
[36] T.J. Yu, J.L. Lippert, W.L. Peticolas, Laser Raman studies of conformational variations of poly-L-lysine, Biopolymers 12 (1973) 2161–2176.
[37] S. Ikeda, Heat-induced gelation of whey proteins observed by rheology, atomic force microscopy, and Raman scattering spectroscopy, Food Hydrocolloids 17 (2003) 399–406.
[38] E.C. Li-Chan, The applications of Raman spectroscopy in food science, Trends Food Sci. Technol. 7 (1996) 361–370.
[39] A. Torreggiani, M. Tamba, I. Manco, M.R. Faraone-Mennella, C. Ferreri, C. Chatgilialoglu, Radiation damage of lysozyme in a biomimetic model: some insights by Raman spectroscopy, J. Mol. Struct. 744 (2005) 767–773.
[40] C. Pérez-Rodriguez, N. Montano, K. Gonzalez, K. Griebenow, Stabilization of α-chymotrypsin at the CH_2Cl_2/water interface and upon water-in-oil-in-water encapsulation in PLGA microspheres, J. Controlled Release 89 (2003) 71–85.